crystals

MDPI

Article

A High Laser Damage Threshold and a Good Second-Harmonic Generation Response in a New Infrared NLO Material: $LiSm_3SiS_7$

Ni Zhen, Leyan Nian, Guangmao Li, Kui Wu * and Shilie Pan *

Key Laboratory of Functional Materials and Devices for Special Environments of CAS, Xinjiang Key Laboratory of Electronic Information Materials and Devices, Xinjiang Technical Institute of Physics & Chemistry of CAS, 40-1 South Beijing Road, Urumqi 830011, China; zhenni50@163.com (N.Z.); nianleyan@163.com (L.N.); lgm559271@163.com (G.L.)

* Correspondence: wukui@ms.xjb.ac.cn (K.W.); slpan@ms.xjb.ac.cn (S.P.); Tel.: +86-991-3674558 (S.P.)

Academic Editor: Helmut Cölfen

Received: 29 June 2016; Accepted: 19 September 2016; Published: 23 September 2016

Abstract: A series of new infrared nonlinear optical (IR NLO) materials, $LiRe_3MS_7$ (Re = Sm, Gd; M = Si, Ge), have been successfully synthesized in vacuum-sealed silica tubes via a high-temperature solid-state method. All of them crystallize in the non-centrosymmetric space group $P6_3$ of the hexagonal system. In their structures, LiS_6 octahedra connect with each other by sharing common faces to form infinite isolated one-dimensional $_\infty[LiS_3]_n$ chains along the 6_3 axis. ReS_8 polyhedra share edges and corners to construct a three-dimensional tunnel structure with $_\infty[LiS_3]_n$ chains located inside. Remarkably, $LiSm_3SiS_7$ shows promising potential as one new IR NLO candidate, including a wide IR transparent region (0.44–21 μm), a high laser damage threshold (LDT) (3.7 × benchmark $AgGaS_2$), and a good NLO response (1.5 × $AgGaS_2$) at a particle size between 88 μm and 105 μm. Dipole-moment calculation was also used to analyze the origin of NLO responses for title compounds.

Keywords: nonlinear optical materials; crystal structure; good NLO responses

1. Introduction

Nonlinear optical (NLO) crystals play an increasingly critical role in developing new coherent light sources by frequency conversion technology on traditional lasers [1,2]. Recently, numerous famous NLO crystals have been discovered and have effectively solved the generation of UV-visible light [3–22]. However, for the mid-far infrared (IR) region (3–20 μm), outstanding IR NLO materials have been discovered less, and only a few (chalcopyrites $AgGaS_2$, $AgGaSe_2$, and $ZnGeP_2$) have been commercially applied [23–25]. Note that some of the self-defects hinder their future development (especially for high-energy laser system), such as low laser-damage thresholds (LDTs) for $AgGaS_2$ and $AgGaSe_2$, and serious two-photon absorption (TPA) for $ZnGeP_2$. Nowadays, the development of many important fields, such as laser guidance, infrared remote sensing, and telecommunication, has hardly been realized without the help of high-energy IR sources. Thus, to find new excellent IR NLO materials with a wide IR transparent range, a good chemical stability, a high LDT, and a large NLO coefficient is still an urgent task and a great challenge. In recent decades, research systems have almost covered the entire periodic table, and hundreds of new IR NLO crystals have been discovered [26–52]. As one NLO material, a non-centrosymmetric (NCS) structure is an essential condition. Previous investigations indicate that tetrahedral $M^{IV}S_4$ (M^{IV} = Si, Ge, and Sn) with lively alkali metals can increase the opportunity to obtain NCS structures [53,54]. Moreover, combining the electropositive elements including alkaline, alkaline-earth, or rare-earth metals with crystal structures can increase the band gaps of compounds and further increase their LDTs [55,56]. Based on the above strategy, we have focused our research interests on the Li−Re−M−S system and fortunately obtained

three new NCS compounds: $LiSm_3SiS_7$, $LiSm_3GeS_7$, and $LiGd_3GeS_7$, which belong to the well-known ARe_3MQ_7 family, where A is the monovalent, divalent, or trivalent ions, Re is the rare-earth ions, M is the tetravalent ions (Si^{4+}, Ge^{4+}, and Sn^{4+}), and Q is S or Se [57–64]. To the best of our knowledge, Li-containing ARe_3MQ_7 compounds has not been reported yet. All of them crystallize in the polar space groups of $P6_3$ and exhibit similar crystal structures. Among them, $LiSm_3SiS_7$ has a high laser damage threshold about 3.7 times that of benchmark $AgGaS_2$. In addition, $LiSm_3SiS_7$ also shows a wide transmission window in the IR range (up to 21 μm) and a large NLO response (1.5 × $AgGaS_2$) at a particle size between 88 μm and 105 μm. Herein, $LiSm_3SiS_7$ can be expected as a new NLO candidate in the IR region.

2. Results and Discussion

2.1. Crystal Structure

Three compounds including $LiSm_3SiS_7$, $LiSm_3GeS_7$, and $LiGd_3GeS_7$ crystallize in the NCS polar space group $P6_3$ of the hexagonal system. Herein, $LiSm_3SiS_7$ was chosen as the representative to illuminate its crystal structure. In its asymmetric unit, there is one unique Sm atom, one Li atom, one Si atom, and three S atoms. As for its structure, Sm atoms are connected with eight S atoms to form the distorted SmS_8 polyhedra with d(Sm−S) = 2.791(5) − 2.993(6) Å. SmS_8 polyhedra connect together by sharing corners or edges to form the three-dimensional tunnel framework (Figure 1a). Si atoms are connected with four S atoms to form the isolated typical SiS_4 tetrahedra with d(Si−S) = 2.089(2) − 2.132(1) Å. Li atoms are linked with six S atoms to form LiS_6 octahedra with three short (2.568(8) Å) and three long (2.623(3) Å) Li−S bonds. The LiS_6 octahedra share faces with each other to form one-dimensional $_\infty[LiS_3]_n$ chains along the 6_3 axis, and the chains then stretch in the tunnels surrounded by SmS_8 (Figure 1b,c). In addition, title compounds have similar crystal structures to previous reported ARe_3MQ_7 series of crystals [57–64], where A represents Na, Cu, and Ag. In this work, the new Li-containing compounds were discovered to enlarge the $A^IRe_3M^{IV}Q_7$ family and enrich the structural chemistry.

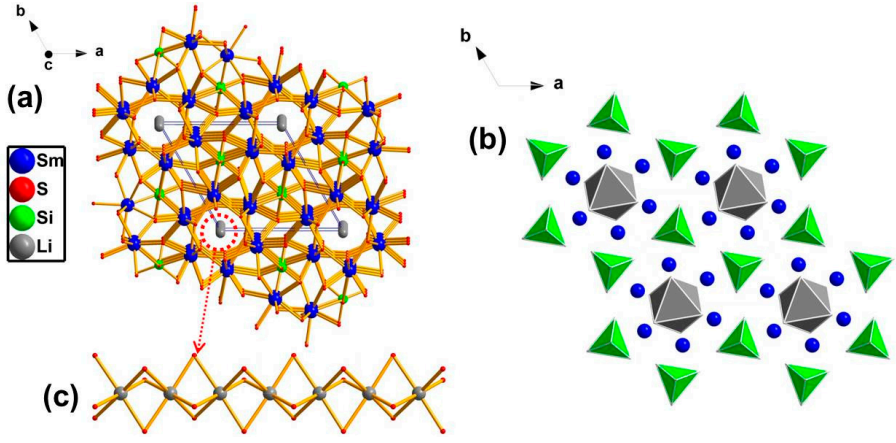

Figure 1. (**a**) Crystal structure of $LiSm_3SiS_7$. All the Li–S bonds are omitted for clarity. (**b**) Structure of $LiSm_3SiS_7$ viewed down the c-axis. The Sm−S bonds were omitted for the sake of clarity. Blue: Sm; Gray octahedron: LiS_6; Green tetrahedron: SiS_4. (**c**) One-dimensional $_\infty[LiS_3]_n$ chains in $LiSm_3SiS_7$.

Moreover, in order to ensure the reasonability of crystal structures of these compounds, the bond valence [65,66] and the global instability index (GII) [67–69] are systemically calculated (Table 1). The method of bond-valence parameters was used to calculate the bond valences of elements. The following equation is commonly used to calculate the bond valence (v_{ij}):

$$V_i = \sum_j v_{ij} = \sum_j \exp\left(\frac{r' - r_{ij}}{B}\right), \quad (1)$$

where *r'* is an empirically determined bond valence parameter, r_{ij} is the actual bond length, and B is commonly taken to be a universal constant equal to 0.37 Å. Calculated results (Li, 0.993–1.021; Sm/Gd, 3.024–3.039; Si/Ge, 4.060–4.134; S, 1.933–2.128) indicate that all atoms are in reasonable oxidation states. In addition, GII can be derived from the bond valence concepts, which represent the tension of lattice parameters and are always used to evaluate the rationality of structure. While the value of GII is less than 0.05 vu (valence unit), the tension of the structure is not proper; while the value of GII is larger than 0.2 vu, its structure is not stable. Thus, the value of GII in a reliable structure should be limited to 0.05–0.2 in general. As for title compounds, calculated GII values are in the range of 0.07–0.09 vu, which illustrates that the crystal structures of all compounds are reasonable.

Table 1. Bond valence sum (vu) and global instability index (GII) of title compounds.

Compounds	Li^+	Sm/Gd^{3+}	Si/Ge^{4+}	S^{2-}	GII
$LiSm_3SiS_7$	1.019	3.039	4.060	1.962–2.106	0.07
$LiSm_3GeS_7$	0.993	3.034	4.114	1.933–2.102	0.08
$LiGd_3GeS_7$	1.021	3.024	4.134	1.936–2.128	0.09

2.2. Optical Properties

Experimental optical bandgap (Figure 2) of $LiSm_3SiS_7$ was measured to be 2.83 eV (440 nm), which is consistent with the crystal color (pale yellow). IR and Raman spectra (Figure 2) show that $LiSm_3SiS_7$ has a wide transmission range in the IR region (up to 21 μm) that covers two critical atmospheric windows (3–5 and 8–12 μm), which is comparable to those reported for powdered $BaGa_4Se_7$ (~18 μm) [35], $AgGaS_2$ (~23 μm) [30], Li_2CdGeS_4 (~22 μm) [70], and $Na_2Hg_3Si_2S_8$ (~20 μm) [47]. Moreover, the bandgap (2.83 eV) of $LiSm_3SiS_7$ is larger than that of commercial $AgGaS_2$ crystal (2.56 eV) [30]; thus, $LiSm_3SiS_7$ may have a higher laser damage resistance since the LDT is generally proportional to the bandgap for one material. In this work, a pulse laser (1.06 μm, 10 Hz, and 10 ns) was chosen to measure the LDT of $LiSm_3SiS_7$ with $AgGaS_2$ as the reference on powder samples (Table 2). The LDT value of $LiSm_3SiS_7$ is 118 MW/cm^2, about 3.7 times that of commercial $AgGaS_2$ (32 MW/cm^2), which shows this material has good potential to apply in the high-power laser system. We have also investigated the second-harmonic generation (SHG) response for $LiSm_3SiS_7$, and the particle size versus SHG intensity of $LiSm_3SiS_7$ indicates a nonphase-matching behavior at 2.09 μm. As seen from Figure 3 and Table 3, $LiSm_3SiS_7$ shows a large SHG response about 1.5 times that of standard $AgGaS_2$ in the 88–105 μm particle size range. Remarkably, $LiSm_3SiS_7$ also achieves a suitable balance of high LDT and good SHG response, which can effectively avoid the drawbacks (low LDT and harmful TPA) of commercially available materials. Thus, $LiSm_3SiS_7$ has potential application as a NLO material in the mid- and far-IR region.

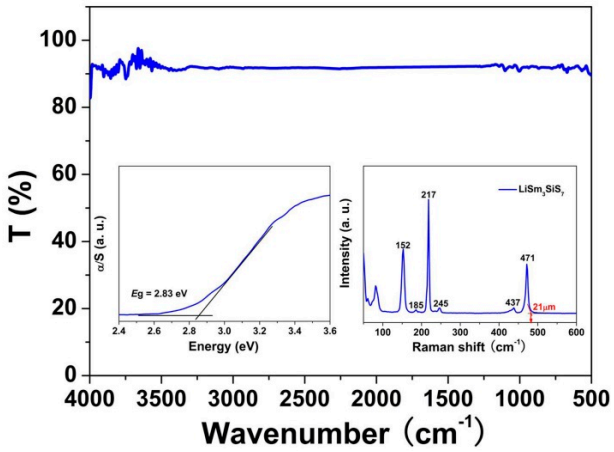

Figure 2. Optical properties (infrared (IR), bandgap, and Raman) of $LiSm_3SiS_7$.

Table 2. Laser-damage thresholds (LDTs) of $LiSm_3SiS_7$ and $AgGaS_2$ (as the reference).

Compounds	Damage Energy (mJ)	Spot Diameter (mm)	LDT (MW/cm^2)
$AgGaS_2$	0.35	0.375	32
$LiSm_3SiS_7$	0.58	0.25	118

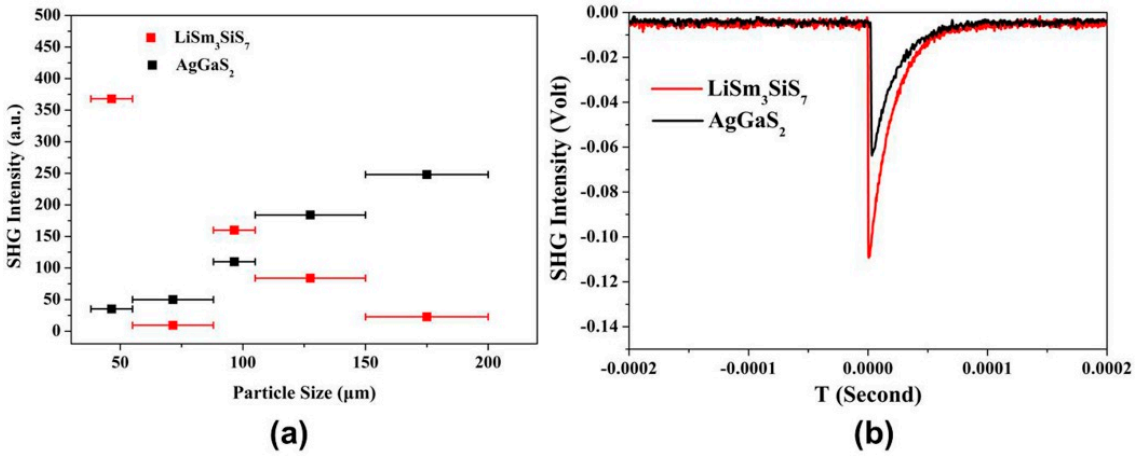

Figure 3. (**a**) Second-harmonic generation (SHG) intensity versus particle size for $LiSm_3SiS_7$ and $AgGaS_2$. (**b**) Comparison on SHG intensities for $LiSm_3SiS_7$ and $AgGaS_2$ at the particle size (88–105 μm).

Table 3. SHG intensity versus particle size for $LiSm_3SiS_7$ and $AgGaS_2$ (as the reference).

	Particle Size (μm)				
compounds	33–55	55–88	88–105	105–150	150–200
$AgGaS_2$	35.2	50	110	185	248
$LiSm_3SiS_7$	368	9.4	163	84	23

2.3. Dipole Moment Calculation

The SHG response has a close relationship with the distortion degree of anionic groups in the crystal structure. While the spatial arrangement of all units tends to be uniform, the local NLO effects stack with each other, and then lead to a large NLO effect for material. Thus, in order to obtain a deeper understanding of NLO responses origin of title compounds, the dipole moments for the [LiS_6], [ReS_8], and [MS_4] units were calculated with a bond-valence method [71–73], and the calculated results are listed in Table 4. From the table, it can be seen that the polarizations of the x- and y-directions from all building units are almost canceled out, and the polarizations of z-direction are constructively added in a unit cell for title compounds. Moreover, the polarization of the [ReS_8] unit is also found to be much larger than those of the distorted [LiS_6] octahedra and [MS_4] tetrahedra for all title compounds. As seen from the results for previous reported $La_3Ga_{0.5}(Ge_{0.5}/Ga_{0.5})S_7$ and $La_3In_{0.5}(Ge_{0.5}/In_{0.5})S_7$ on the calculation of cutoff-energy-dependent SHG coefficient [57], their SHG responses mainly originate from the transition processes from S-3p, La-5d states to La-5d, S-3p states, which are consistent with the calculated results of dipole moments for the title compounds in this work.

Table 4. Dipole moment calculations for $LiRe_3MS_7$ (Re = Sm, Gd; M = Si, Ge).

Species	Dipole Moment				
	x (a)	*y* (b)	*z* (c)	Magnitude	
				Debye	$\times 10^{-4}$ esu·cm/Å^3
$LiSm_3SiS_7$					
LiS_6	0.00	0.00	9.52	9.52	0.04
SmS_8	0.00	0.06	21.08	21.08	0.09
SiS_4	0.00	0.00	−8.24	8.24	0.03
Unit cell	0.00	0.06	22.37	22.37	0.09
$LiSm_3GeS_7$					
LiS_6	0.00	0.00	8.23	8.23	0.03
SmS_8	0.06	0.00	21.31	24.90	0.10
GeS_4	0.00	0.00	−8.05	8.05	0.03
Unit cell	0.06	0.00	21.49	21.49	0.09
$LiGd_3GeS_7$					
LiS_6	0.00	0.00	14.06	14.06	0.06
GdS_8	0.00	0.00	22.18	26.91	0.12
GeS_4	0.00	0.00	−8.43	8.43	0.04
Unit cell	0.00	0.00	27.81	27.81	0.12

3. Materials and Methods

3.1. Synthesis

Raw materials were commercially purchased. Because Li metal is easily oxidized in air, all the preparation processes were completed in an Ar-filled glovebox.

3.1.1. $LiSm_3SiS_7$

Elementary reactants of Li, Sm, Si, and S were weighted at the stoichiometric ratio of 1:3:1:7. All the raw materials were firstly loaded into a graphite crucible, the graphite crucible was then put into a silica tube, and the tube was flame-sealed under 10^{-3} Pa. The detailed temperature-setting curve for the muffle furnace was heated to 850 °C in 50 h and kept at this temperature for about 100 h, then slowly cooled to 300 °C by 80 h, finally quickly cooled to the room temperature. The product was washed with *N*,*N*-dimethylformamide (DMF) to remove the byproducts. Pale-yellow crystals were found and stable in the air.

3.1.2. $LiSm_3GeS_7$ and $LiGd_3GeS_7$

These reaction processes including starting composition and heating profile are similar to that of $LiSm_3SiS_7$. Finally, yellow crystals were also obtained by washing with DMF, but they would deliquesce when exposed to air for a long time.

3.2. Structure Determination

Selected high-quality crystals were used for data collections on a Bruker SMART APEX II 4K CCD diffractometer (Bruker Corporation, Madison, WI, USA) using MoKα radiation (λ = 0.71073 Å) at 296 K. The crystal structures were solved by a direct method and refined using the SHELXTL program package [74]. Multi-scan method was chosen for absorption correction [75]. As for the $LiSm_3SiS_7$, the space group was determined from the systematic absences was $P6_3$. The first run of a routine refinement of the initial structure generated an "un-balanced" formula of "Sm_3SiS_7" with R_1 = 2.04%, R_2 = 5.06%. In addition, a high electron density peak with 6.49 e$^-$/Å^3 and 2.55 Å away from S1, was observed. We also tried to assign this position to the other atoms or a mixed occupation with two atoms (Li and Sm), but no refinement results were proper or obtained the balanced formula. Only this position was assigned as Li1, which provided a balanced formula of "$LiSm_3SiS_7$," and R_1 and R_2

converged to improved values of 1.50% and 3.05%. Rational anisotropic thermal parameters for all atoms were obtained by the anisotropic refinement and extinction correction. Moreover, the maximum and minimum peaks on the final Fourier difference map corresponded to 0.57 and −0.60 $e^-/Å^3$. Other two compounds ($LiSm_3GeS_7$ and $LiGd_3GeS_7$) have the similar refinement process with that of $LiSm_3SiS_7$. Final structures were also checked with the PLATON program, and no other symmetries were found. Crystallographic data for title compounds are reported in Table 5.

Table 5. Crystal data and structure refinement for $LiRe_3MS_7$ (Re = Sm, Gd; M = Si, Ge).

Empirical Formula	$LiSm_3SiS_7$	$LiSm_3GeS_7$	$LiGd_3GeS_7$
Formula weight	710.50	755.00	775.70
Temperature		296 (2) K	
Crystal system		Hexagonal	
Space group		$P6_3$	
Unit cell dimensions	a = 10.007(2) Å c = 5.668(3) Å	a = 9.991(3) Å c = 5.752(3) Å	a = 9.900(7) Å c = 5.753(5) Å
Z, *V*	2, 491.6(3) $Å^3$	2, 497.3(4) $Å^3$	2, 488.4(2) $Å^3$
Density (calculated)	4.800 g/cm^3	5.042 g/cm^3	5.274 g/cm^3
crystal size (mm^3)	0.182 × 0.180 × 0.095	0.261 × 0.172 × 0.138	0.210 × 0.160 × 0.120
Completeness to theta = 27.49	100 %	100.0 %	100 %
Goodness-of-fit on F^2	1.003	1.183	1.150
Final *R* indices $[F_o^2 > 2\sigma(F_o^2)]$ [a]	R_1 = 0.0150 wR_2 = 0.01558	R_1 = 0.0162 wR_2 = 0.0169	R_1 = 0.0179 wR_2 = 0.0180
R indices (all data) [a]	R_1 = 0.0303 wR_2 = 0.0305	R_1 = 0.0357 wR_2 = 0.0359	R_1 = 0.0399 wR_2 = 0.0399
Absolute structure parameter	0.02(2)	0.011(18)	−0.02 (2)
Extinction coefficient	0.0150(3)	0.0277(6)	0.0350(8)
Largest diff. peak and hole	0.564 and −0.614 e $Å^{-3}$	0.661 and −0.648 e $Å^{-3}$	1.052 and −1.291 e $Å^{-3}$

[a] $R_1 = F_o - F_c/F_o$ and $wR_2 = [w(F_o^2 - F_c^2)^2/wF_o^4]^{1/2}$ for $F_o^2 > 2\sigma(F_o^2)$.

3.3. Powder XRD Measurement

Powder X-ray diffraction (XRD) analysis was measured at room temperature using an automated Bruker D2 X-ray diffractometer. However, we did not prepare the pure phase of $LiSm_3GeS_7$ and $LiGd_3GeS_7$ for the reason of moisture absorption. In this work, only the pure phase of $LiSm_3SiS_7$ was obtained, and we systemically studied its physicochemical properties. In addition, in comparison with calculated and experiment results (Figure 4), it can be found that the experimental powder XRD patterns are basically consistent with calculated values.

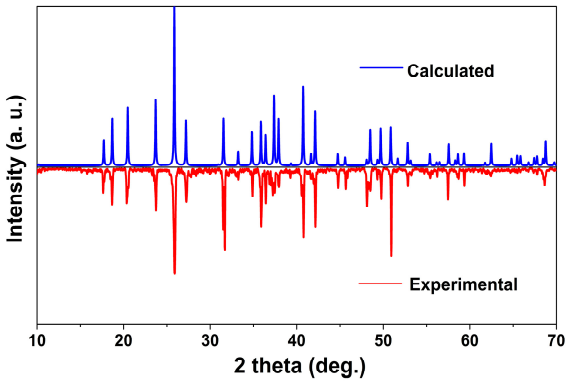

Figure 4. Powder X-ray diffraction (XRD) patterns of $LiSm_3SiS_7$.

3.4. UV–Vis–NIR Diffuse-Reflectance Spectroscopy

With a Shimadzu SolidSpec-3700DUV spectrophotometer, optical diffuse reflectance spectrum was measured in the wavelength range from 190 nm to 2600 nm. The absorption spectrum was calculated from the diffuse reflectance spectra according to the Kubelka–Munk function: $\alpha/S = (1 - R)^2/2R$, where R is the reflectance coefficient, and α and S are the absorption and scattering coefficient, respectively. Based on the absorption spectrum, the optical bandgap was obtained with the absorption edge of material.

3.5. Raman Spectroscopy

Hand-picked single-crystals were put on an object slide, and a LABRAM HR Evolution spectrometer (Shimadzu Corporation, Beijing, China) equipped with a CCD detector with a 532-nm laser was then used to record the Raman spectra. The integration time was 5 s.

3.6. Infrared Spectroscopy

IR spectra were measured on the powder sample mixed with dried KBr powder. A Shimadzu IRAffinity-1 Fourier transform infrared spectrometer recorded the measurement data in the range of 400–4000 cm^{-1} with a resolution of 2 cm^{-1}.

3.7. Second-Harmonic Generation (SHG) Measurement

A Q-switch laser (2.09 μm, 3 Hz, 50 ns) was used to measure the SHG response with different particle sizes on powder sample, including 38–55, 55–88, 88–105, 105–150, and 150–200 μm. The $AgGaS_2$ crystal was ground and sieved into the same size ranges as the reference.

3.8. LDT Measurement

A pulse laser (1.06 μm, 10 Hz, and 10 ns) was chosen to estimate the powder LDT with the same powdered $AgGaS_2$ sample as the reference with a particle size range of 150–200 μm. The detail test procedure is as follows: with increasing laser energy, the color change of the powder sample was constantly observed with an optical microscope to determine the damage threshold. To adjust different laser beams, an optical concave lens was added into the laser path. The damage spot was measured by the scale of optical microscope.

3.9. Calculations of Group Dipole Moments

The dipole moments of the LiS_6, SmS_8, GdS_8, SiS_4, and GeS_4 units were calculated with a simple bond-valence method [71–73]. Distribution of the electron on the each atom was estimated by the bond-valence theory $v_{ij} = \exp[(r' - r_{ij})/B$; where r' is the empirical constant, r_{ij} is the actual bond length, and B is commonly taken to be a universal constant equal to 0.37 Å. The geometrical position was taken from the unit cell of the experimental X-ray crystal structure. The Debye equation $\mu = neR$, where μ is the net dipole moment in Debye, n the total number of electrons, e the charge on an electron, and R the difference, in cm, between the "centroids" of positive and negative charges, was used to calculate the dipole moment.

4. Conclusions

In summary, the first three new Li-containing ARe_3MQ_7 compounds including $LiSm_3SiS_7$, $LiSm_3GeS_7$, and $LiGd_3GeS_7$ are isostructural with a polar space group $P6_3$ in the hexagonal system. The $LiSm_3SiS_7$, for example, features a 3D tunnel structure composed of isolated SiS_4 tetrahedra, 1D $_\infty[LiS_3]_n$ chains along the 6_3 axis formed by face-sharing LiS_6 octahedra, and 3D framework by the interconnection of SmS_8 polyhedra, with the 1D $_\infty[LiS_3]_n$ chains located in the tunnels. Moreover, $LiSm_3SiS_7$ shows good SHG efficiency ~1.5 times that of $AgGaS_2$ in the particle size range of 88–105 μm and a high LDT that is ~3.7 times that of $AgGaS_2$, demonstrating that $LiSm_3SiS_7$ exhibits a suitable

balance of good SHG response and high LDT and can be expected to be a potential candidate in the IR NLO region.

Supplementary Materials: The following are available online at http://www.mdpi.com/2073-4352/6/10/121/s1. Cifs for title compounds.

Acknowledgments: This work was supported by Natural Science Foundation of Xinjiang, China (Grant No. 2014211B046).

Author Contributions: Ni Zhen and Leyan Nian contributed equally. Ni Zhen conceived and designed this study, prepared the crystals, and wrote the manuscript. Leyan Nian carried out the properties characterization work and analysis. Guangmao Li analyzed the crystal structures. Kui Wu and Shilie Pan conceived and coordinated the project.

Conflicts of Interest: The authors declare no conflict of interest.

References

1. Duarte, F.J. *Tunable Laser Applications*, 2nd ed.; CRC Press: Boca Raton, FL, USA, 2008; Chapters 2, 9, and 12.
2. Nikogosyan, D.N. *Nonlinear Optical Crystals: A Complete Survey*, 1st ed.; Springer: New York, NY, USA, 2005.
3. Chen, C.T.; Wu, Y.C.; Jiang, A.D.; Wu, B.C.; You, G.M.; Li, R.K.; Lin, S.J. New Nonlinear-Optical Crystal: LiB_3O_5. *J. Opt. Soc. Am. B* **1989**, *6*, 616–621. [CrossRef]
4. Chen, C.T.; Wu, B.C.; Jiang, A.D.; You, G.M. A New-Type Ultraviolet SHG Crystal-β-BaB_2O_4. *Sci. Sin. Ser. B (Engl. Ed.)* **1985**, *28*, 235–243.
5. Mei, L.; Wang, Y.; Chen, C.T.; Wu, B.C. Nonlinear Optical Materials Based on $MBe_2BO_3F_2$ (M = Na, K). *J. Appl. Phys.* **1993**, *74*, 7014–7016. [CrossRef]
6. Wang, G.L.; Zhang, C.Q.; Chen, C.T.; Yao, A.Y.; Zhang, J.; Xu, Z.Y.; Wang, J.Y. High-Efficiency 266-nm Output of A $KBe_2BO_3F_2$ Crystal. *Appl. Opt.* **2003**, *42*, 4331–4334. [CrossRef] [PubMed]
7. Becker, P. Borate Materials in Nonlinear Optics. *Adv. Mater.* **1998**, *10*, 979–992. [CrossRef]
8. Sun, C.F.; Hu, C.L.; Xu, X.; Ling, J.B.; Hu, T.; Kong, F.; Long, X.F.; Mao, J.G. $BaNbO(IO_3)_5$: A New Polar Material with A Very Large SHG Response. *J. Am. Chem. Soc.* **2009**, *131*, 9486–9487. [CrossRef] [PubMed]
9. Hu, C.L.; Mao, J.G. Recent Advances on Second-Order NLO Materials Based on Metal Iodates. *Coord. Chem. Rev.* **2015**, *288*, 1–17. [CrossRef]
10. Song, J.L.; Hu, C.L.; Xu, X.; Kong, F.; Mao, J.G. A Facile Synthetic Route to a New SHG Material with Two Types of Parallel π-Conjugated Planar Triangular Units. *Angew. Chem. Int. Ed.* **2015**, *54*, 3679–3682. [CrossRef] [PubMed]
11. Zou, G.H.; Ye, N.; Huang, L.; Lin, X.S. Alkaline-Alkaline Earth Fluoride Carbonate Crystals $ABCO_3F$ (A = K, Rb, Cs; B = Ca, Sr, Ba) as Nonlinear Optical Materials. *J. Am. Chem. Soc.* **2011**, *133*, 20001–20007. [CrossRef] [PubMed]
12. Yang, G.S.; Peng, G.; Ye, N.; Wang, J.Y.; Luo, M.; Yan, T.; Zhou, Y.Q. Structural Modulation of Anionic Group Architectures by Cations to Optimize SHG Effects: A Facile Route to New NLO Materials in the $ATCO_3F$ (A = K, Rb; T = Zn, Cd) Series. *Chem. Mater.* **2015**, *27*, 7520–7530. [CrossRef]
13. Zou, G.H.; Huang, L.; Ye, N.; Lin, C.S.; Cheng, W.D.; Huang, H. $CsPbCO_3F$: A Strong Second-Harmonic Generation Material Derived from Enhancement via p$-\pi$ Interaction. *J. Am. Chem. Soc.* **2013**, *135*, 18560–18566. [CrossRef] [PubMed]
14. Yu, H.W.; Zhang, W.G.; Young, J.; Rondinelli, J.M.; Halasyamani, P.S. Bidenticity-Enhanced Second Harmonic Generation from Pb Chelation in $Pb_3Mg_3TeP_2O_{14}$. *J. Am. Chem. Soc.* **2016**, *138*, 88–91. [CrossRef] [PubMed]
15. Yu, H.W.; Zhang, W.G.; Young, J.; Rondinelli, J.M.; Halasyamani, P.S. Design and Synthesis of the Beryllium-Free Deep-Ultraviolet Nonlinear Optical Material $Ba_3(ZnB_5O_{10})PO_4$. *Adv. Mater.* **2015**, *27*, 7380–7385. [CrossRef] [PubMed]
16. Kim, H.G.; Tran, T.T.; Choi, W.; You, T.S.; Halasyamani, P.S.; Ok, K.M. Two New Non-centrosymmetric $n = 3$ Layered Dion–Jacobson Perovskites: Polar $RbBi_2Ti_2NbO_{10}$ and Nonpolar $CsBi_2Ti_2TaO_{10}$. *Chem. Mater.* **2016**, *28*, 2424–2432. [CrossRef]
17. Zou, G.H.; Nam, G.; Kim, H.G.; Jo, H.; You, T.S.; Ok, K.M. $ACdCO_3F$ (A = K and Rb): New Noncentrosymmetric Materials with Remarkably Strong Second-Harmonic Generation (SHG) Responses Enhanced via π-Interaction. *RSC Adv.* **2015**, *5*, 84754–84761. [CrossRef]

18. Cheng, L.; Wei, Q.; Wu, H.Q.; Zhou, L.J.; Yang, G.Y. $Ba_3M_2[B_3O_6(OH)]_2[B_4O_7(OH)_2]$ (M = Al, Ga): Two Novel UV Nonlinear Optical Metal Borates Containing Two Types of Oxoboron Clusters. *Chem.—Eur. J.* **2013**, *19*, 17662–17667. [CrossRef] [PubMed]
19. Huang, H.W.; Liu, L.J.; Jin, S.F.; Yao, W.J.; Zhang, Y.H.; Chen, C.T. Deep-Ultraviolet Nonlinear Optical Materials: $Na_2Be_4B_4O_{11}$ and $LiNa_5Be_{12}B_{12}O_{33}$. *J. Am. Chem. Soc.* **2013**, *135*, 18319–18322. [CrossRef] [PubMed]
20. Li, F.; Hou, X.L.; Pan, S.L.; Wang, X.A. Growth, structure, and optical properties of a congruent melting oxyborate, $Bi_2ZnOB_2O_6$. *Chem. Mater.* **2009**, *21*, 2846–2850. [CrossRef]
21. Wu, H.P.; Pan, S.L.; Poeppelmeier, K.R.; Li, H.Y.; Jia, D.Z.; Chen, Z.H.; Fan, X.Y.; Yang, Y.; Rondinelli, J.M.; Luo, H.S. $K_3B_6O_{10}Cl$: A New Structure Analogous to Perovskite with a Large Second Harmonic Generation Response and Deep UV Absorption Edge. *J. Am. Chem. Soc.* **2011**, *133*, 7786–7790. [CrossRef] [PubMed]
22. Yu, H.W.; Wu, H.P.; Pan, S.L.; Yang, Z.H.; Hou, X.L.; Su, X.; Jing, Q.; Poeppelmeier, K.R.; Rondinelli, J.M. $Cs_3Zn_6B_9O_{21}$: A Chemically Benign Member of the KBBF Family Exhibiting the Largest Second Harmonic Generation Response. *J. Am. Chem. Soc.* **2014**, *136*, 1264–1267. [CrossRef] [PubMed]
23. Okorogu, A.O.; Mirov, S.B.; Lee, W.; Crouthamel, D.I.; Jenkins, N.; Dergachev, A.Y.; Vodopyanov, K.L.; Badikov, V.V. Tunable Middle Infrared Downconversion in GaSe and $AgGaS_2$. *Opt. Commun.* **1998**, *155*, 307–312. [CrossRef]
24. Boyd, G.D.; Storz, F.G.; McFee, J.H.; Kasper, H.M. Linear and Nonlinear Optical Properties of Some Ternary Selenides. *IEEE J. Quantum Electron.* **1972**, *8*, 900–908. [CrossRef]
25. Boyd, G.D.; Buehler, E.; Storz, F.G. Linear and Nonlinear Optical Properties of $ZnGeP_2$ and CdSe. *Appl. Phys. Lett.* **1971**, *18*, 301–304. [CrossRef]
26. Chung, I.; Kanatzidis, M.G. Metal chalcogenides: A rich source of nonlinear optical materials. *Chem. Mater.* **2014**, *26*, 849–869. [CrossRef]
27. Jiang, X.M.; Guo, S.P.; Zeng, H.Y.; Zhang, M.J.; Guo, G.C. Large Crystal Growth and New Crystal Exploration of Mid-Infrared Second-Order Nonlinear Optical Materials. *Struct. Bond.* **2012**, *145*, 1–43.
28. Bera, T.K.; Jang, J.I.; Ketterson, J.B.; Kanatzidis, M.G. Strong Second Harmonic Generation from the Tantalum Thioarsenates $A_3Ta_2AsS_{11}$ (A = K and Rb). *J. Am. Chem. Soc.* **2009**, *131*, 75–77. [CrossRef] [PubMed]
29. Zhang, W.; Li, F.; Kim, S.H.; Halasyamani, P.S. Top-Seeded Solution Crystal Growth and Functional Properties of A Polar Material $Na_2TeW_2O_9$. *Cryst. Growth Des.* **2010**, *10*, 4091–4095. [CrossRef]
30. Lin, H.; Zhou, L.J.; Chen, L. Sulfides with Strong Nonlinear Optical Activity and Thermochromism: $ACd_4Ga_5S_{12}$ (A = K, Rb, Cs). *Chem. Mater.* **2012**, *24*, 3406–3414. [CrossRef]
31. Chen, M.C.; Wu, L.M.; Lin, H.; Zhou, L.J.; Chen, L. Disconnection Enhances the Second Harmonic Generation Response: Synthesis and Characterization of $Ba_{23}Ga_8Sb_2S_{38}$. *J. Am. Chem. Soc.* **2012**, *134*, 6058–6060. [CrossRef] [PubMed]
32. Yu, P.; Zhou, L.J.; Chen, L. Noncentrosymmetric Inorganic Open-Framework Chalcohalides with Strong Middle IR SHG and Red emission: $Ba_3AGa_5Se_{10}Cl_2$ (A = Cs, Rb, K). *J. Am. Chem. Soc.* **2012**, *134*, 2227–2235. [CrossRef] [PubMed]
33. Chen, M.C.; Li, L.H.; Chen, Y.B.; Chen, L. In-Phase Alignments of Asymmetric Building Units in Ln_4GaSbS_9 (Ln= Pr, Nd, Sm, Gd−Ho) and Their Strong Nonlinear Optical Responses in Middle IR. *J. Am. Chem. Soc.* **2011**, *133*, 4617–4624. [CrossRef] [PubMed]
34. Chen, Y.K.; Chen, M.C.; Zhou, L.J.; Chen, L.; Wu, L.M. Syntheses, Structures, and Nonlinear Optical Properties of Quaternary Chalcogenides: $Pb_4Ga_4GeQ_{12}$ (Q = S, Se). *Inorg. Chem.* **2013**, *52*, 8334–8341. [CrossRef] [PubMed]
35. Yao, J.Y.; Mei, D.J.; Bai, L.; Lin, Z.S.; Yin, W.L.; Fu, P.Z.; Wu, Y.C. $BaGa_4Se_7$: A New Congruent-Melting IR Nonlinear Optical Material. *Inorg. Chem.* **2010**, *49*, 9212–9216. [CrossRef] [PubMed]
36. Lin, X.S.; Zhang, G.; Ye, N. Growth and Characterization of $BaGa_4S_7$: A New Crystal for Mid-IR Nonlinear Optics. *Cryst. Growth Des.* **2009**, *9*, 1186–1189. [CrossRef]
37. Luo, Z.Z.; Lin, C.S.; Cui, H.H.; Zhang, W.L.; Zhang, H.; Chen, H.; He, Z.Z.; Cheng, W.D. $PbGa_2MSe_6$ (M = Si, Ge): Two Exceptional Infrared Nonlinear Optical Crystals. *Chem. Mater.* **2015**, *27*, 914–922. [CrossRef]
38. Luo, Z.Z.; Lin, C.S.; Cui, H.H.; Zhang, W.L.; Zhang, H.; He, Z.Z.; Cheng, W.D. SHG Materials $SnGa_4Q_7$ (Q = S, Se) Appearing with Large Conversion Efficiencies, High Damage Thresholds, and Wide Transparencies in the Mid-Infrared Region. *Chem. Mater.* **2014**, *26*, 2743–2749. [CrossRef]

39. Geng, L.; Cheng, W.D.; Lin, C.S.; Zhang, W.L.; Zhang, H.; He, Z.Z. Syntheses and Characterization of New Mid-Infrared Transparency Compounds: Centric Ba_2BiGaS_5 and Acentric Ba_2BiInS_5. *Inorg. Chem.* **2011**, *50*, 5679–5686. [CrossRef] [PubMed]
40. Luo, Z.Z.; Lin, C.S.; Zhang, W.L.; Zhang, H.; He, Z.Z.; Cheng, W.D. $Ba_8Sn_4S_{15}$: A Strong Second Harmonic Generation Sulfide with Zero-Dimensional Crystal Structure. *Chem. Mater.* **2013**, *26*, 1093–1099. [CrossRef]
41. Liu, B.W.; Zeng, H.Y.; Zhang, M.J.; Fan, Y.H.; Guo, G.C.; Huang, J.S.; Dong, Z.C. Syntheses, Structures, and Nonlinear-optical Properties of Metal Sulfides $Ba_2Ga_8MS_{16}$ (M = Si, Ge). *Inorg. Chem.* **2014**, *54*, 976–981. [CrossRef] [PubMed]
42. Li, S.F.; Liu, B.W.; Zhang, M.J.; Fan, Y.H.; Zeng, H.Y.; Guo, G.C. Syntheses, Structures, and Nonlinear Optical Properties of Two Sulfides $Na_2In_2MS_6$ (M = Si, Ge). *Inorg. Chem.* **2016**, *55*, 1480–1485. [CrossRef] [PubMed]
43. Wu, Q.; Meng, X.G.; Zhong, C.; Chen, X.G.; Qin, J.G. $Rb_2CdBr_2I_2$: A New IR Nonlinear Optical Material with A Large Laser Damage Threshold. *J. Am. Chem. Soc.* **2014**, *136*, 5683–5686. [CrossRef] [PubMed]
44. Zhang, G.; Li, Y.J.; Jiang, K.; Zeng, H.Y.; Liu, T.; Chen, X.G.; Qin, J.G.; Lin, Z.S.; Fu, P.Z.; Wu, Y.C.; et al. A New Mixed Halide, $Cs_2HgI_2Cl_2$: Molecular Engineering for a New Nonlinear Optical Material in the Infrared Region. *J. Am. Chem. Soc.* **2012**, *134*, 14818–14822. [CrossRef] [PubMed]
45. Haynes, A.S.; Saouma, F.O.; Otieno, C.O.; Clark, D.J.; Shoemaker, D.P.; Jang, J.I.; Kanatzidis, M.G. Phase-Change Behavior and Nonlinear Optical Second and Third Harmonic Generation of the One-Dimensional $K_{(1-x)}Cs_xPSe_6$ and Metastable β-$CsPSe_6$. *Chem. Mater.* **2015**, *27*, 1837–1846. [CrossRef]
46. Wu, K.; Yang, Z.H.; Pan, S.L. $Na_4MgM_2Se_6$ (M = Si, Ge): The First Noncentrosymmetric Compounds with Special Ethane-Like $[M_2Se_6]^{6-}$ Units Exhibiting Large Laser-Damage Thresholds. *Inorg. Chem.* **2015**, *54*, 10108–10110. [CrossRef] [PubMed]
47. Wu, K.; Yang, Z.H.; Pan, S.L. $Na_2Hg_3M_2S_8$ (M = Si, Ge, and Sn): New Infrared Nonlinear Optical Materials with Strong Second Harmonic Generation Effects and High Laser-Damage Thresholds. *Chem. Mater.* **2016**, *28*, 2795–2801. [CrossRef]
48. Wu, K.; Yang, Z.H.; Pan, S.L. Na_2BaMQ_4 (M = Ge, Sn; Q = S, Se): Infrared Nonlinear Optical Materials with Excellent Performances and that Undergo Structural Transformations. *Angew. Chem. Int. Ed.* **2016**, *128*, 6825–6827. [CrossRef]
49. Pan, M.Y.; Ma, Z.J.; Liu, X.C.; Xia, S.Q.; Tao, X.T.; Wu, K.C. $Ba_4AgGa_5Pn_8$ (Pn = P, As): New Pnictide-Based Compounds with Nonlinear Optical Potential. *J. Mater. Chem. C* **2015**, *3*, 9695–9700. [CrossRef]
50. Kuo, S.M.; Chang, Y.M.; Chung, I.; Jang, J.I.; Her, B.H.; Yang, S.H.; Ketterson, J.B.; Kanatzidis, M.G.; Hsu, K.F. New Metal Chalcogenides $Ba_4CuGa_5Q_{12}$ (Q = S, Se) Displaying Strong Infrared Nonlinear Optical Response. *Chem. Mater.* **2013**, *25*, 2427–2433. [CrossRef]
51. Bera, T.K.; Jang, J.I.; Song, J.H.; Malliakas, C.D.; Freeman, A.J.; Ketterson, J.B.; Kanatzidis, M.G. Soluble Semiconductors $AAsSe_2$ (A = Li, Na) with A Direct-Band-Gap and Strong Second Harmonic Generation: A Combined Experimental and Theoretical Study. *J. Am. Chem. Soc.* **2010**, *132*, 3484–3495. [CrossRef] [PubMed]
52. Liao, J.H.; Marking, G.M.; Hsu, K.F.; Matsushita, Y.; Ewbank, M.D.; Borwick, R.; Cunningham, P.; Rosker, M.J.; Kanatzidis, M.G. α- and β- $A_2Hg_3M_2S_8$ (A = K, Rb; M = Ge, Sn): Polar Quaternary Chalcogenides with Strong Nonlinear Optical Response. *J. Am. Chem. Soc.* **2003**, *125*, 9484–9493. [CrossRef] [PubMed]
53. Parthé, E. *Crystal Chemistry of Tetrahedral Structures*; Gordon and Breach Science: New York, NY, USA, 1964.
54. Aitken, J.A.; Larson, P.; Mahanti, S.D.; Kanatzidis, M.G. Li_2PbGeS_4 and Li_2EuGeS_4: Polar Chalcopyrites with a Severe Tetragonal Compression. *Chem. Mater.* **2001**, *13*, 4714–4721. [CrossRef]
55. Bai, L.; Lin, Z.S.; Wang, Z.Z.; Chen, C.T. Mechanism of Linear and Nonlinear Optical Effects of Chalcopyrites $LiGaX_2$ (X = S, Se, and Te) Crystals. *J. Appl. Phys.* **2008**, *103*, 083111. [CrossRef]
56. Kim, Y.; Seo, I.S.; Martin, S.W.; Baek, J.; Shiv Halasyamani, P.; Arumugam, N.; Steinfink, H. Characterization of New Infrared Nonlinear Optical Material with High Laser Damage Threshold, $Li_2Ga_2GeS_6$. *Chem. Mater.* **2008**, *20*, 6048–6052. [CrossRef]
57. Shi, Y.F.; Chen, Y.K.; Chen, M.C.; Wu, L.M.; Lin, H.; Zhou, L.J.; Chen, L. Strongest Second Harmonic Generation in the Polar R_3MTQ_7 Family: Atomic Distribution Induced Nonlinear Optical Cooperation. *Chem. Mater.* **2015**, *27*, 1876–1884. [CrossRef]
58. Rudyk, B.W.; Stoyko, S.S.; Mar, A. Rare-earth transition-metal indium sulphides RE_3FeInS_7 (RE = La–Pr), RE_3CoInS_7 (RE = La, Ce), and La_3NiInS_7. *J. Solid State Chem.* **2013**, *208*, 78–85. [CrossRef]

59. Choudhury, A.; Dorhout, P.K. Alkali-Metal Thiogermanates: Sodium Channels and Variations on the La_3CuSiS_7 Structure Type. *Inorg. Chem.* **2015**, *54*, 1055–1065. [CrossRef] [PubMed]
60. Poduska, K.M.; DiSalvo, F.J.; Min, K.; Halasyamani, P.S. Structure Determination of La_3CuGeS_7 and $La_3CuGeSe_7$. *J. Alloys Compd.* **2002**, *335*, 5–9. [CrossRef]
61. Hwu, S.J.; Bucher, C.K.; Carpenter, J.D.; Taylor, S.P. A Solid-state Diastereomer, $AgLa_3GeS_7$. *Inorg. Chem.* **1995**, *34*, 1979–1980. [CrossRef]
62. Gulay, L.D.; Olekseyuk, I.D.; Wołcyrz, M.; Stepien-Damm, J. The Crystal Structures of R_3CuSnS_7 (R = La–Nd, Sm, Gd–Ho). *Z. Anorg. Allg. Chem.* **2005**, *631*, 1919–1923. [CrossRef]
63. Gulay, L.D.; Lychmanyuk, O.S.; Olekseyuk, I.D.; Daszkiewicz, M.; Stepien-Damm, J.; Pietraszko, A. Crystal Structures of the Compounds R_3CuSiS_7 (R = Ce, Pr, Nd, Sm, Tb, Dy and Er) and $R_3CuSiSe_7$ (R = La, Ce, Pr, Nd, Sm, Gd, Tb and Dy). *J. Alloys Compd.* **2007**, *431*, 185–190. [CrossRef]
64. Yin, W.L.; Shi, Y.G.; Kang, B.; Deng, J.G.; Yao, J.Y.; Wu, Y.C. Rare-Earth Transition-Metal Chalcogenides Ln_3MGaS_7 (Ln = Nd, Sm, Dy, Er; M = Co, Ni) and Ln_3MGaSe_7 (Ln = Nd, Sm, Gd, Dy, M = Co; Ln = Nd, Gd, Dy, M = Ni). *J. Solid State Chem.* **2014**, *213*, 87–92. [CrossRef]
65. Brese, N.E.; O'Keeffe, M. Bond-Valence Parameters for Solid. *Acta Crystallogr. B* **1991**, *47*, 192–197. [CrossRef]
66. Brown, I.D.; Altermatt, D. Bond-Valence Parameters Obtained from a Systematic Analysis of the Inorganic Crystal Structure Database. *Acta Crystallogr. B* **1985**, *41*, 244–247. [CrossRef]
67. Brown, I.D. *The Chemical Bond in Inorganic Chemistry: The Bond Valence Model*, 1st ed.; Oxford University Press: Oxford, UK, 2002.
68. Preiser, C.; Losel, J.; Brown, I.D.; Kunz, M.; Skowron, A. Long Range Coulomb Forces and Localized Bonds. *Acta Crystallogr. B* **1999**, *55*, 698–711. [CrossRef] [PubMed]
69. Salinas-Sanchez, A.; Garcia-Munoz, J.L.; Rodriguez-Carvajal, J.; Saez-Puche, R.; Martinez, J.L. Structural Characterization of R_2BaCuO_5 (R = Y, Lu, Yb, Tm, Er, Ho, Dy, Gd, Eu and Sm) Oxides by X-ray and Neutron Diffraction. *J. Solid State Chem.* **1992**, *100*, 201–211. [CrossRef]
70. Brant, J.A.; Clark, D.J.; Kim, Y.S.; Jang, J.I.; Zhang, J.H.; Aitken, J.A. Li_2CdGeS_4, A Diamond-Like Semiconductor with Strong Second-Order Optical Nonlinearity in the Infrared and Exceptional Laser Damage Threshold. *Chem. Mater.* **2014**, *26*, 3045–3048. [CrossRef]
71. Maggard, P.A.; Nault, T.S.; Stern, C.L.; Poeppelmeier, K.R. Alignment of Acentric $MoO_3F_3^{3-}$ Anions in a Polar Material: $(Ag_3MoO_3F_3)(Ag_3MoO_4)Cl$. *J. Solid State Chem.* **2003**, *175*, 27–33. [CrossRef]
72. Ok, K.M.; Halasyamani, P.S. Mixed-Metal Tellurites: Synthesis, Structure, and Characterization of $Na_{1.4}Nb_3Te_{4.9}O_{18}$ and $NaNb_3Te_4O_{16}$. *Inorg. Chem.* **2005**, *44*, 3919–3925. [CrossRef] [PubMed]
73. Kim, J.H.; Halasyamani, P.S. A Rare Multi-Coordinate Tellurite, $NH_4ATe_4O_9{\cdot}2H_2O$ (A = Rb or Cs): The Occurrence of TeO_3, TeO_4, and TeO_5 Polyhedra in the Same Material. *J. Solid State Chem.* **2008**, *181*, 2108–2112. [CrossRef]
74. Sheldrick, G.M. *SHELXTL*; Version 6.14; Bruker Analytical X-ray Instruments, Inc.: Madison, WI, USA, 2008.
75. Spek, A.L. Single-Crystal Structure Validation with the Program PLATON. *J. Appl. Crystallogr.* **2003**, *36*, 7–13. [CrossRef]